2016

Cyclic lateral response of FRP-confined circular concrete-filled steel tubular columns

Tao Yu
University of Wollongong, taoy@uow.edu.au

Y M. Hu
Hong Kong Polytechnic University, AECOM Asia Co. Ltd.

Jin Guang Teng
Hong Kong Polytechnic University, cejgteng@polyu.edu.hk

Publication Details

Yu, T., Hu, Y. M. & Teng, J. G. (2016). Cyclic lateral response of FRP-confined circular concrete-filled steel tubular columns. Journal of Constructional Steel Research, 124 12-22.

Cyclic lateral response of FRP-confined circular concrete-filled steel tubular columns

Abstract
Concrete-filled steel tubular (CFT) columns are widely used as columns in many structural systems and a common failure mode of such tubular columns is inelastic outward local buckling near a column end. The use of fibre-reinforced polymer (FRP) jackets/wraps for the suppression of such local buckling has recently been proposed and has been proven to possess excellent potential in both retrofit/strengthening and new construction. This paper presents the results of an experimental study into the behaviour of large-scale FRP-confined CFT (CCFT) columns under combined axial compression and lateral loading. The test parameters included the stiffness of the FRP jacket and the loading scenario. The test results showed that the FRP jacket can effectively delay or even prevent outward local buckling at the end of a cantilevered CFT column, leading to significantly improved structural performance under combined constant axial compression and cyclic lateral loading. Compared to monotonic lateral loading, cyclic lateral loading was found to introduce more severe localized deformation near the column end and may lead to earlier FRP rupture within that region.

Keywords
confined, columns, cyclic, lateral, tubular, response, frp, steel, filled, concrete, circular

Publication Details
Yu, T., Hu, Y. M. & Teng, J. G. (2016). Cyclic lateral response of FRP-confined circular concrete-filled steel tubular columns. Journal of Constructional Steel Research, 124 12-22.

BEHAVIOUR OF FRP-CONFINED CIRCULAR CONCRETE-FILLED STEEL TUBULAR COLUMNS SUBJECTED TO COMBINED AXIAL COMPRESSION AND CYCLIC LATERAL LOADING

T. Yu[1], Y.M. Hu[2] and J.G. Teng[3*]

ABSTRACT

Concrete-filled steel tubular (CFT) columns are widely used as columns in many structural systems and a common failure mode of such tubular columns is inelastic outward local buckling near a column end. The use of fibre-reinforced polymer (FRP) jackets/wraps for the suppression of such local buckling has recently been proposed and has been proven to possess excellent potential in both retrofit/strengthening and new construction. This paper presents the results of an experimental study into the behaviour of large-scale FRP-confined CFT (CCFT) columns under combined axial compression and lateral loading. The test parameters included the stiffness of the FRP jacket and the loading scenario. The test results showed that the FRP jacket can effectively delay or even prevent outward local buckling at the end of a cantilevered CFT column, leading to significantly improved structural performance under combined constant axial compression and cyclic lateral loading. Compared to monotonic lateral loading, cyclic lateral loading was found to introduce more severe localized deformation near the column end and may lead to earlier FRP rupture within that region.

INTRODUCTION

Concrete-filled steel tubular (CFT) columns are widely used as columns in many structural systems. In CFT columns, inward buckling deformations of the steel tube are prevented by the concrete core, but degradation in steel confinement, strength and ductility can result from inelastic outward local buckling. In practice, columns are normally subjected to not only axial compression but also lateral loads, such as wind and seismic loads. Extensive studies have been conducted on CFT columns under combined axial and lateral loads (e.g. [1-3]). In such columns, the critical regions are the ends of the column where the moments are the largest. Under seismic loading, large plastic rotations without significant degradation in stiffness and strength are demanded at these critical regions. Against this background, Xiao [4] proposed a novel form of CFT columns, named by him as confined CFT (or CCFT) columns in which the end portions are confined with steel tube segments or fiber-reinforced polymer (FRP) wraps. In these columns, due to the additional confinement from an FRP or steel segment, both the inward and the outward buckling deformations of the steel tube are constrained, so the ductility and strength of the column can be substantially enhanced in the end regions. In addition, the concrete is better confined with the additional confinement from the FRP or steel segment [4, 5]. Such FRP confinement of CFTs can be exploited in structural

[1] Senior Lecturer, School of Civil, Mining and Environmental Engineering, Faculty of Engineering and Information Sciences, University of Wollongong, Northfields Avenue, Wollongong, NSW 2522, Australia.
[2] Project Engineer, AECOM Asia Co. Ltd. and formerly, PhD Student, Department of Civil and Environmental Engineering, The Hong Kong Polytechnic University, Hong Kong, China.
[3] Ko Jan Ming Professor in Sustainable Structures and Materials and Chair Professor of Structural Engineering, Department of Civil and Environmental Engineering, The Hong Kong Polytechnic University, Hong Kong, China (Corresponding Author). Email: cejgteng@polyu.edu.hk

strengthening for enhanced strength and ductility, and in new construction for more ductile and economical structures [6].

Following Xiao's initial work [4], a number of studies have been conducted by Xiao and his associates (e.g. [7-9]) as well as other researchers (e.g. [10-16]) on the effectiveness of FRP confinement in improving the structural behaviour of CFT columns. The authors' group has conducted a systematic study into the axial compressive behavior of FRP-confiend circular CFT columns; this study included several series of tests on cicular glass FRP (GFRP)-confined CFT columns under monotonic axial compression [6] and cyclic axial compression [17], and the development of monotonic and cyclic stress-strain models for the confined concrete in circular CCFT columns [17, 18].

Despite the significant amount of existing research on the axial compressive behavior of CCFT columns, the experimental research on its seismic behavior has been very limited. The limited existing studies [7-9, 14], have generally confirmed the excellent seismic resistance of circular [8, 9] and square CCFTs [7, 14]. In this paper, a series of large-scale cantilever column tests are presented, where CFT columns with or without FRP jacketing at the column end were tested under combined constant axial compression and monotonic or cyclic lateral loading. The test programme was designed to develop a good understanding of the behaviour of such CCFT columns, and to examine the effects of two important test parameters, namely, the stiffness/type of the FRP jacket and the loading scenario (i.e. monotonic lateral loading and cyclic lateral loading). To the best knowledge of the authors, no existing studies have examined both of the two parameters in a systemtic manner. The details of the specimens and the test set-up are first presented, followed by the presentation and discussion of the test observations and results.

EXPERIMENTAL PROGRAMME

Details of Specimens

In total five large-scale columns were prepared and tested, among which two were tested under combined axial compression and monotonic lateral loading (referred to as type E loading hereafter), while the other three were tested under combined axial compression and cyclic lateral loading (referred to as type F loading hereafter). The two columns tested under type E loading included one CFT specimen as the control specimen and one CCFT specimen with a five-ply glass (GFRP) jacket. The three columns tested under type F loading included two specimens which were nominally identical to the two tested under type E loading so that the effect of loading scenarios can be examined; they also included an additional CCFT specimen with a six-ply carbon FRP (CFRP) jacket so that the effect of FRP jacket stiffness can be examined. All the five columns had a circular section with a diameter of 318 mm, and a height of 1625 mm from the point of lateral loading to the top of the stiff reinforced concrete (RC) footing which was 1500 mm long, 1400 mm wide and 550 mm thick. The steel tubes used in all specimens had a thickness of 3 mm, leading to a D_{outer}/t_s ratio of 106. For the three CCFT specimens, an FRP jacket was applied to provide additional confinement to the potential plastic hinge region which was assumed to be 500 mm from the column footing. The details of all specimens are summarized in Table 1.

Preparation of Specimens

All specimens were constructed at the Structural Engineering Research Laboratory of The

Hong Kong Polytechnic University. Each specimen consisted of a CFT or a CCFT column with one end embedded in a stiff RC footing. In the preparation process, the steel tube of the column was connected to the steel reinforcement embedded in the RC footing in the following way: (1) the steel tube was first welded to a bottom steel plate which was 700 mm long, 500 wide and 25 mm thick; the steel tube was centralized on the steel plate; (2) six vertical stiffeners were then welded to the embedded part of the steel tube (i.e. the part within the RC footing); each stiffener had a radial width of 120 mm, a thickness of 20 mm and a height of 480 mm ; (3) a 20 mm thick and 100 mm wide steel ring which was formed from two halves was then placed onto the stiffeners and welded to the steel tube; the steel ring was used to ensure a uniform stress distribution at the end of the column (i.e. the part above the footing). The steel tube integrated with the embedded steel reinforcement is shown in Figure 1. The steel assembly was next enclosed in a wooden formwork for the casting of concrete to form the footing which was heavily reinforced to ensure a sufficiently large stiffness/strength (Figure 2). Afterwards, commercially available concrete was cast both in the steel tube and to form the footing. One week later, a thin layer of gypsum was applied on the top surface of the concrete in the steel tube to eliminate the gap between the top surface of the concrete and the top end of the steel tube caused by the shrinkage of concrete, so that the two components can be axially-loaded simultaneously in the test.

The FRP jacket was formed via a wet lay-up process, and each ply consisted of a single lap of a fibre sheet impregnated with an epoxy resin. A continuous fibre sheet was wrapped around the steel tube to form a jacket with the required number of plies, with the finishing end of the fibre sheet overlapping its starting end by 150 mm to ensure circumferential stress transfer. Before the wrapping of the FRP jacket, the surface of the steel tube was properly cleaned using alcohol. The height of the FRP jacket was finally 490 mm instead of the designed 500 mm for ease of installing transducers.

Material Properties

Three concrete cylinders were prepared for each column according to Ref. [19] and tested according to Ref. [20] in order to determine the cylinder strength, the axial strain at peak axial stress, and the elastic modulus of concrete. The so-obtained concrete properties are summarized in Table 2. Three steel coupons were cut from a steel tube which was from the same batch as those in the columns and tested according to Ref. [21]. The steel had an elastic modulus of 203 GPa, a yield stress of 271 MPa, and an ultimate stress of 353 MPa. The GFRP jacket used had an elastic modulus of 80.1 GPa and an ultimate strain of 2.28%, based on a nominal thickness of 0.17 mm per ply. These GFRP material properties are taken from the coupon tests presented in Ref. [17] where the same batch of glass fiber sheets was used. The CFRP jacket used had an elastic modulus of 237.8 GPa and an ultimate strain of 0.85%, based on a nominal thickness of 0.34 mm per ply as obtained from five tensile coupon tests following Ref. [22]. The adhesive had an elastic modulus of 1.7 GPa and an ultimate tensile stress of 55 MPa according to the manufacturer.

Instrumentation

In order to monitor the behaviour of the column, extensive strain gauging and many LVDTs were employed in the test of each column as summarized below.

A number of bi-directional strain gauges were used to measure the axial and hoop strain distributions of the column at five different column heights, namely, the circumferences at 20

mm, 150 mm, 325 mm, 470 mm and 850 mm from the column footing top surface respectively. For each of the three lower heights, eight strain gauges were evenly installed around the circumference. The other two heights (i.e. at 470 mm and 850 mm) were expected to be outside the plastic hinge region, so a smaller number (i.e. four) of strain gauges were used for each circumference and they were placed at 90 degrees apart from each other. The gauge length of the strain gauges attached to the steel tubes was 10 mm while that of the strain gauges attached onto the FRP jackets was 20 mm. The layout of the strain gauges is shown in Figure 3. For ease of reference, the five cross-sections where strain gauges were attached are defined as Sections A to E from the column bottom end (Figure 3).

Eight pairs of linear variable displacement transducers (LVDTs) were installed on the two sides of the loading plane (i.e. the western side and the eastern side, see Figure 4) of the column at intervals of 100 mm starting from the column end (i.e. the top surface of the footing). These LVDTs were installed on the column surface through pre-fixed nuts (Figure 5). The eight segments with LVDTs attached are referred to as the first to the eighth segments from the column end. In addition, two pairs of LVDTs (each pair consisted of one vertical and one horizontal transducer) were used on the two sides of the foundation to monitor the movement it might experience during the test. Two LVDTs were installed at the column head to measure the lateral displacement. The rotation of the column head and the shortening of the column were also measured by LVDTs. The layout of the LVDTs is shown in Figure 4.

Testing Frame

All the tests were conducted using a testing frame which is capable of testing large-scale structural members and sub-assemblies at the Structural Engineering Research Laboratory of The Hong Kong Polytechnic University. Figure 6 shows a photo of the testing frame while Figure 7 shows a schematic diagram of the test set-up for the present columns. The testing frame (Figures 6 and 7) includes a vertical actuator (capacity: 3,000 kN in tension and 10,000 kN in compression) connected to a relatively large plate (i.e. top plate) and a hinge joint connected to a relatively small plate (i.e. bottom plate); rollers are provided between the top plate and the bottom plate so that during the test the horizontal locations of the actuator and the hinge can be adjusted. In addition, a horizontal actuator (capacity: 1,000 kN in tension and 1,500 kN in compression) is provided which can apply horizontal loading through a hinge joint. The positions of both actuators can be controlled manually. In the test, the specimen was fixed to a strong floor using eight sets of screws (80 mm in diameter) and nuts. Both hinges were lubricated in advance to minimize the friction force during the test.

In the test, significant frictional forces were induced between the top and the bottom plates (see Figure 7) because of the large axial load applied to the column and the relative movement between the two plates when the column was horizontally pulled or pushed. These frictional forces need to be deducted from the load readings of the horizontal actuator to obtain the horizontal load actually resisted by the column. In the present study, the frictional forces were determined in the following way: (1) a certain displacement was applied to the column head while the position of the axial actuator was held; in this process, the direction of frictional forces acting on the column was opposite to that of the applied displacement; (2) an equal displacement was applied to the axial actuator while the position of column head was held; in this process, the direction of frictional forces acting on the column was the same as that of the applied displacement. This change of direction of the frictional forces led to changes in the load readings of the horizontal actuator. The magnitude of the frictional forces was therefore taken to be half of the difference between the load readings of process (1) and

process (2). In each column test, many pairs of processes (1) and (2) were executed, and the frictional forces during each test were averaged from the values found from the many pairs of processes (1) and (2). The so-obtained frictional forces for all column tests are summarized in Table 3. The frictional coefficients for different specimens are seen to be similar (Table 3), indirectly confirming the reliability of these results. The average frictional coefficient is 0.00527.

Loading Scheme

A constant axial load N_{35} which is equal to 35% of the column squash load N_{sq} was applied to each column. N_{35} is given by the following equation:

$$N_{35} = 0.35N_{sq} = 0.35(f_y A_s + f'_{co} A_c) \quad (1)$$

where f_y and A_s are the yield stress and the cross-sectional area of the steel tube respectively; f'_{co} is the cylinder compressive strength of concrete; and A_c is the cross-sectional area of the concrete core. It should be noted that for different columns, the concrete strengths were slightly different (Table 2), so the magnitudes of the applied constant axial load were also slightly different (Table 3).

Following the practice of many existing studies (e.g. [23-25]), the lateral loading was applied step by step based on the yield displacement of the column. The yield displacement of the column was defined in the following way which was suggested as by Priestly and Park [26]: (1) load the column to a level which is 0.75 times the maximum lateral load H_{peak}; H_{peak} was estimated through a sectional analysis method adopting the stress-strain model developed in Ref. [18] for the confined concrete and a column analysis method for evaluating the column behaviour [27]; (2) the yield displacement δ_y is defined as the elastic limit of an equivalent elastic-perfectly plastic curve with a reduced stiffness being equal to the secant stiffness at 75% of the peak lateral load (i.e. $0.75H_{peak}$; see Figure 8). For the columns subjected to cyclic lateral loading, the yield displacement was averaged from the two values found using the method above for the pull direction and the push direction respectively. The so-obtained yield displacements are summarized in Table 4. The cyclic loading schemes were based on these in-situ determined yield displacements and consisted of two cycles at displacement levels of $\pm\delta_y$; $\pm2\delta_y$; $\pm3\delta_y$; $\pm5\delta_y$; $\pm7\delta_y$; $\pm9\delta_y$ and one cycle at displacement levels of $\pm11\delta_y$ (Figure 9), except for specimen LCFT-0-106-F where the second cycle at $\pm9\delta_y$ was not performed due to time limitation. It should be noted that in the above descriptions the term "displacement" or "lateral displacement" refers to the lateral displacement at the column head. This simplification in terminology is also used elsewhere in this paper unless otherwise specified.

In the present study, no fatal brittle failure occurred in all the cantilever tests, even though the FRP jacket ruptured and the steel tube fractured in specimen LCFT-5G-106-F. Hence, the two monotonic loading tests were terminated when the lateral resistance of the column was reduced to a reasonably low level; for the other columns which were loaded cyclically, the tests were terminated after the pre-determined loading scheme had been completed (Figure 9).

At such a large final lateral displacement (i.e. $\pm 11\delta_y$), the lateral resistance of the column was reduced significantly.

TEST OBSERVATIONS

The two specimens without an FRP jacket (i.e. specimens LCFT-0-106-E, F) showed localized outward buckling deformation at a lateral displacement of around 20 mm (Figure 10). The first local buldge for both specimens was located at a height of around 60 mm from the column end, and developed with the increase of displacement. For the cyclically loaded specimen (i.e. specimen LCFT-0-106-F), the bulges on both sides of the steel tube formed a ring around the column (Figure 10b). In the later stage of loading, a smaller bulge was noticed in each specimen at a height of around 250 mm from the column end (Figure 10a). Readings from axial strain gauges revealed that the plane section assumption was generally valid for the higher sections (Figure 11a). For the lower sections, the strain distributions were approximately linear at lower displacement levels, but became significantly nonlinear afterwards (Figure 11b) when the strain distributions were significantly affected by localized deformations such as concrete cracks on the tension side and bulges on the compression side of the steel tube. A similar conclusion can also be made for the specimens with an FRP jacket. The hoop strains were found to be generally higher for a lower section where the moment was larger, except for section A (i.e. the lowest section) where only limited hoop strains were developed because of the constraint from the column end (Figure 12a).

The localized outward buckling of steel tube was found to be significantly delayed by the GFRP jacket. For specimen LCFT-5G-106-E which was under monotonic loading, a local bulge beame noticeable only at a displacement of 80 mm, and no severe damage of the GFRP jacket was found except for a few tensile cracks in the resin (Figure 13a). For the nominally identical specimen under cyclic loading (i.e. LCFT-5G-106-F), however, the failure process was much more complicated: initial tensile cracks in the resin occurred on both sides of the tube at a displacement of around 25 mm; the opening of these cracks led to reduced confinement to the steel tube when the column was loaded in the opposite direction, so the bulges appeared earlier (i.e. at a displacement of around 50 mm) in this specimen. The locations of the bulges in the two specimens (i.e. around 30 mm from the column end) were both found to be lower than that in the corresponding CFT specimen, leading to large hoop strains at Section A (Figure 12b). The bulges in specimen LCFT-5G-106-F led to major tensile cracks at approximately the same location, which could not be closed in the subsequent loading cycle because of the localized lateral expansion caused by the previous bulge. Consquently, damage of the GFRP jacket in this region became increasingly severe, and finally led to hoop tensile rupture of the jacket (Figure 13b).

For specimen LCFT-6C-106-F where a much stronger CFRP jacket was used, the outward local buckling of steel tube was almost prevented. Within the region wrapped with CFRP, only a slight bulge could be felt by hand, which did not become more apparent with the displacement. Instead, a larger bulge appeared above the CFRP-wrapped zone in the later stage of loading (Figure 14). No rupture of the CFRP jacket was found during the test.

TEST RESULTS AND DISCUSSIONS

General

The detailed test results are presented and discussed in this section. For clarity of presentation,

the push direction (i.e. western direction) is defined to be the positive direction while the pull direction (i.e. eastern direction) is defined to be the negative direction (Figure 7); compressive stresses/strains are defined to be negative while tensile strains/stresses are defined to be positive. These definitions are adopted throughout this paper unless otherwise specified. Therefore, for example, the western side of a column is in compression and the eastern side is in tension when a column is loaded in the push (positive) direction.

Normalized Moment-Curvature Curves

The concrete strengths of the different columns are slightly different (see Table 2). To minimize the effect of the differences in concrete strength, the test results of different columns were normalized before being compared. Table 2 shows that columns LCFT-0-106-E and LCFT-5G-106-F (referred to as group I) had approximately the same concrete strength while the concrete strengths of columns LCFT-5G-106-E, LCFT-0-106-F and LCFT-6C-106-F (referred to as group II) were very close. In the present study, the bending moments resisted by a column are normalized by the peak moment of the CFT column of the same group.

The curvature of a section is commonly found from strains at different locations of the section. In the present study, the strains obtained from the LVDT readings were used instead of those obtained from the axial strain gauges as the latter cover only a small vertical distance (i.e. 20 mm or 10mm) and their readings were more easily affected by localized deformations. With the LVDT readings, the average curvature of a segment is given by:

$$\phi_{\Delta} = \frac{(\Delta_1 - \Delta_2)}{D' l_{seg}} \tag{2}$$

where ϕ_{Δ} is the average curvature of the segment based on LVDT readings; l_{seg} is the length of the segment; Δ_1 and Δ_2 are the LVDT readings on the western and eastern sides of the segment respectively; D' is the horizontal distance between the tips of the two transducers and is slightly larger than the diameter of the column.

The normalized moment-curvature curves of the first segment (i.e. bottom segment) are shown in Figure 15 for all the columns. For the cyclically-loaded columns, two curves are given for loading in both directions. It should be noted that the curvature of a column section may also be affected by the different concrete properties, but this effect is expected to be minor, as also indicated by the very similar initial slopes of the curves shown in Figure 15.

Normalized Lateral Load-Displacement Curves

Besides the concrete strength, the lateral load resisted by a column is affected by the magnitude of the applied axial load because of the second-order effect. In the present study, the axial load applied to a column was equal to 35% of its squash load (Eq. 1) which is also dependent on the concrete strength and is different from one column to another (see Table 3). The second-order effect induced by the applied axial load is therefore also different for different columns. To eliminate the difference in the second-order effect on the lateral load-displacement behaviour, the lateral loads resisted by all the columns were adjusted using the following equation:

$$P_{adj} = P_{ori} + P_{\text{mod}} = P_{ori} + \frac{\left(N_{app} - 1134\right)\delta}{l_{col}} \tag{3}$$

in which, P_{adj} is the adjusted lateral load; P_{ori} is original lateral load from the test readings; N_{app} is the applied axial load; P_{mod} is a value used to consider the different second-order effects in different columns and is equal to zero for column LCFT-0-106-E for which the applied axial load is equal to 1134 kN; l_{col} is the effective length of the column (from the point of loading to the fixed end); and δ is the lateral displacement. The adjusted lateral loads are then normalized by the load P_{nor} which corresponds to the moment used to normalize the bending moments:

$$P_{nor} = \frac{M_{co}}{l_{col}} \tag{4}$$

in which M_{co} is the peak moment of the CFT column of the same group. The normalized load-normalized displacement curves using the above method are shown in Figure 16 for all the columns, where the lateral displacement is normalized by the column length.

Effect of Loading Scenario

The effect of loading scenarios is obvious from the failure modes of the two CCFTs with a GFRP jacket but subjected to monotonic lateral loading and cyclic lateral loading respectively. As described earlier, in the column subjected to monotonic lateral loading (i.e. column LCFT-5G-106-E), the local buckling of the steel tube was significantly delayed and no FRP rupture on the compression side occurred at the end of test. However, in the column subjected to cyclic lateral loading (i.e. column LCFT-5G-106-F), the FRP jacket ruptured on both sides and severe local bulking of the steel tube occurred at the location of FRP rupture (Figure 13b). This suggests that cyclic loading tends to produce more localized deformation near the column end and FRP jacketing may be less effective. However, it should be noted that although this local FRP rupture is a direct consequence of cyclic lateral loading, it can be avoided when the stiffness/strength of the FRP jacket is sufficiently large, as seen from the test results of column LCFT-6C-106-F.

The more severe localized deformation is clearly illustrated in Figure 17 where the curvature distributions of the two CCFT columns (i.e. columns LCFT-5G-106-E and LCFT-5G-106-F) at several displacement levels are compared. It is clear from Figure 17 that at the same displacement level, the curvature are more localized in the first segment (i.e. bottom segment) for the cyclically-loaded column. Similarly observison could also be made when comparing the two CFT columns.

The more localized deformation in a cyclically-loaded column is due to the cumulative damage in its bottom segment during cyclic loading; the cumulative damage weakens the bottom segment and thus leads to further localization of deformation in this segment. At the same displacement level, for a cyclically-loaded column, the curvature in the bottom segment is larger which generally means more severe damage in this segment and more pronounced degradation in the section capacity. Therefore, it can be expected that the descending branch of the moment-lateral displacement curve is steeper for a cyclically-loaded column. This is evident from Figure 18 which shows that the moment generally decreases more rapidly as the

displacement increases for cyclically-loaded columns. However, for the two CFT columns, the effect of cyclic loading on the curves is seen to be small (Figure 18). This is believed to be due to the very good ductility of the CFT section as shown in Figure 15, which means the moment decreases only slowly as the curvature increases. For the two CCFT columns, the effect of cyclic loading is particularly obvious as seen from the curve for the loading in the positive direction (column LCFT-5G-106-F, see Figure 18). This more obvious effect of cyclic loading is due to the rapid degradation of section capacity after the rupture of the FRP jacket, compared to the original FRP-confined section, as seen from Figure 15. Similar observation can also be made from Figure 16 which shows the normalized lateral load-lateral displacement curves of the two pairs of columns.

Based on the foregoing discussions, it can be expected that the effect of cyclic loading on the moment-lateral displacement curve (or the lateral load-lateral displacement curve) of a column is more pronounced when the moment-curvature curve of its cross-section has a steeper descending branch. It can therefore be expected that for CFT columns with a thinner steel tube, the effect of cyclic loading is more significant. On the other hand, when a weak FRP jacket is used, it is likely to be damaged locally under cyclic loading and thus contributes little to the performance of the CFT column although it may improve the column performance under monotonic loading.

Effect of FRP Confinement

It is shown in Figures 13 and 14 that the FRP jacket can effectively delay (when a 5-ply GFRP jacket was used in the present study) or even prevent (when a 6-ply CFRP jacket was used in the present study) an elephant's foot local buckling failure at the end of a cantilevered CFT column when the column is subjected to both constant axial compression and cyclic lateral loading. In columns with a relatively thick FRP jacket (e.g. 6-ply CFRP jacket in the present study), the buckling deformations can be forced by FRP jacketing to appear above the FRP jacketed region (Figure 14). As a result, the curvature distribution in a CFT column with FRP confinement can be quite different from that in a bare CFT column. Figures 19 and 20 compare the curvature distributions for the two monotonically-loaded columns and the three cyclically-loaded columns respectively. These figures generally reveal that with FRP confinement, the localization of curvature is less pronounced. For column LCFT-6C-106-F, significant localization of deformation occurred above the FRP jacketed region because of the bulges developed there (see Figure 14), which apparently affected the curvature distributions.

It is evident from Figures 15 and 18 that the flexural strength (i.e. moment capacity) of the CFT section can be significantly enhanced by FRP confinement. The enhancement increases with an increase in the stiffness/strength of the FRP jacket. It is also shown that the moment-curvature curves of the CFT section have a descending branch after the peak moment, but with FRP confinement, the moment resisted by the section can continuously increase with the curvature (Figure 15).

Figure 16 shows that that the peak lateral load was enhanced with FRP confinement. In addition, the slope of the descending branch of the load-displacement curve became smaller (i.e. slower rate of decrease in the load) when FRP jacketing was provided. As expected, the effect of FRP jacketing becomes more obvious when the stiffness/strength of the jacket is larger.

The hysteristic load-displacement curves of the three cyclically loaded specimens are shown

in Figure 21. The points corresponding to the peak moment of the first segment in both directions are marked on the curves for specimens LCFT-0-106-F and LCFT-5G-106-F, and it is evident that these points are on the descending branch (i.e. post-peak branch) of the curves. This suggests that the member behaviour of the columns was significantly affected by the second-order effect caused by the large axial load acting on the columns. For the CFT specimen (i.e. specimen LCFT-0-106-F), the pinching effect [23] can be identified by examining the shape of the load-displacement curve when the lateral displacement is close to zero. In specimen LCFT-0-106-F, the pinching effect became obvious after the ring-shaped bulge was formed in the steel tube (i.e. after the first excursion of the $\pm 5\delta_y$ cycle). Due to the existence of a bulge on both sides when the lateral displacement was close to zero, the steel tube was much less effective on the tension side in the subsequent lateral loading process. Therefore, the flexural stiffness of the column was very small at that moment. However, with further loading, the bulge was re-straightened which allowed the steel tube to provide tensile resistance again. As a result, the flexural stiffness started to increase only after a certain lateral displacement (Figure 21a). On the other hand, the pinching effect was well controlled in specimen LCFT-5G-106-F before the GFRP rupture as the steel bulges were constrained by the confinement provided by the GFRP jacket (Figure 21b). For specimen LCFT-6C-106-F, the pinching effect was also well controlled and only became obvious after the bulges appeared above the CFRP jacket (Figure 21c).

The effect of FRP confinement is also examined in terms of the ductility of the columns. The ductility of a member is defined as its ability to sustain inelastic deformations prior to collapse, without a substantial loss of strength. The ductility of a column is generally defined based on the deformation capacity or energy dissipation capacity. The most commonly used parameter appears to be the ductility parameter μ_δ defined by the following equation [28-30]:

$$\mu_\delta = \frac{\delta_u}{\delta_y} \tag{5}$$

where δ_y and δ_u are the yield and ultimate displacements of the column. Various definitions of the yield and ultimate displacements of a column have been proposed by different researchers [31]. In the present study, the yield displacement is defined as the elastic limit of an equivalent elastic-perfectly plastic curve with a reduced stiffness being equal to the secant stiffness at 75% of the peak load following Ref. [26] (Figure 8). The ultimate displacement is defined as the displacement where the lateral load carried by the column has undergone a 20 percent reduction, following the practice of many previous studies (e.g. [24, 26]).

The values of the ductility parameter based on the above definition are summarized in Table 5 for all the columns. It is evident that the ductility parameter generally increases with the provision of an FRP jacket, especially when a strong jacket (e.g. 6-ply CFRP jacket) is provided. In particular, the ductility parameter can be enhanced from around 5.55 for the bare CFT column (i.e. LCFT-0-106-F) to 8.86 for column LCFT-6C-106-F when loaded in the negative direction. It may also be noted that the ductility parameter values for the same column can be quite different when they are calculated based on the envelope load-displacement curves in the two different directions (i.e. positive direction and negative direction). This is due to the asymmetric deformation of the columns: for column LCFT-5G-106-F, the smaller ductility parameter for the positive direction is due to the more severe degradation of FRP confinement on that side; for column LCFT-6C-106-F, the smaller

ductility parameter for the positive direction is due to the more severe local bulge developed in the steel tube above the FRP jacketed region on that side. While these differences were caused by unintended asymmetry of the column tests (e.g. asymmetry in geometry, material properties and load application), the results suggest that if local FRP rupture and local bulges in the steel tube above the FRP jacketed region can be avoided, the ductility of a CFT column can be significantly enhanced by strong FRP jacketing. In practice, local FRP rupture near the column end can be avoided by using a stiffer FRP jacket (e.g. using a 6-ply CFRP jacket for the CFT column examined in the present study) or a more deformable FRP jacket, while local bulges above the FRP jacketed region can be delayed by extending the FRP jacket vertically to cover a longer region.

Besides a larger value of the ductility parameter, it should also be noted that the conditions of CFT columns with and without FRP jacketing can be quite different when the load reduction has reached 20% of the peak load. The structural integrity of the FRP-jacketed columns may be much better as damage in the steel tube is much less severe and the concrete is still being well confined, as seen from the present tests.

Besides the ductility parameter defined by Eq. 5, some researchers (e.g. [24, 32, 33]) have also used the total cumulative dissipated energy to assess column behaviour. The total dissipated energy of a column can generally be represented by the area enclosed by the load-displacement curve. From Figures 16 and 21, it is not difficult to find that the capability of energy dissipation of a CFT column can also be significantly increased with FRP confinement.

CONCLUSIONS

This paper has presented a series of large-scale cantilever column tests, where CFT columns with or without FRP jacketing in the end portion of the column were tested under combined constant axial compression and monotonic or cyclic lateral loading. The results and discussions presented in this paper allow the following conclusions to be made:

1. The FRP jacket can effectively delay or even prevent an elephant's foot local buckling failure at the end of a cantilevered CFT column when the column is subjected to both constant axial compression and cyclic lateral loading. In columns with a relatively thick FRP jacket, the buckling deformations may be forced by FRP jacketing to appear above the FRP jacketed region.
2. The performance of a CFT column can be significantly improved by FRP jacketing. Because of FRP confinement, both the flexural strength of a CFT section and the lateral load-carrying capacity of a CFT column can be significantly enhanced. The ductility and the energy-dissipation capacity of the column, although significantly affected by the second-order effect due to the applied axial load, can also be enhanced with FRP confinement.
3. Cyclic lateral loading introduces more severe localized deformation near the column end and may lead to earlier FRP rupture within that region. The performance of a CCFT column subjected to cyclic lateral loading may not be as good as found from a monotonic lateral loading test.

It should also be noted that the CFT columns tested in the present study already possessed good ductility before FRP jacketing. The effect of FRP jacketing can be expected to be more pronounced when weaker sections (i.e. CFTs with a thinner steel tube) are considered, where

the confinement from the steel tube is smaller and the local buckling problem is more pronounced. Apparently, FRP jacketing is a promising approach for improving the performance of CFT columns, especially for those with an economical thin steel tube.

This paper has been focused on the experimental behaviour of CCFT columns. Future research is needed to develop a theoretical model for predicting their cyclic lateral response. For this purpose, a finite element model employing beam-column elements and the fibre element method of section analysis can be developed based on the cyclic stress-strain model presented in Ref. [17].

ACKNOWLEGEMNTS

The authors are grateful for the financial support provided by the Research Grants Council of the Hong Kong Special Administrate Region (PolyU 5269/05E), the National Basic Research Program of China (i.e. the 973 Program) (Project No.: 2012CB026201), and the Australian Research Council through a Discovery Early Career Researcher Award (Project ID: DE140101349) for the first author.

REFERENCES

[1] Ichinohe, Y., Matsutani, T., Nakajima, M., Ueda, H., and Takada, K. "Elasto-plastic behavior of concrete filled steel circular columns." *Proceedings, Third International Conference on Steel-Concrete Composite Structures*, Fukuoka, Japan, 1991; 131-136.

[2] Han, L.H., and Yang, Y.F. "Cyclic performance of concrete-filled steel CHS columns under flexural loading." *Journal of Constructional Steel Research*, 2005; 61(4), 423-452.

[3] Valipour, H.R., and Foster, S.J. "Nonlinear static and cyclic analysis of concrete-filled steel columns." *Journal of Constructional Steel Research*, 2010; 66(6), 793-802.

[4] Xiao, Y. "Applications of FRP composites in concrete columns." *Advances in Structural Engineering*, 2004; 7(4), 335-343.

[5] Teng, J.G., Yu, T. And Fernando, D. “Strengthening of steel structures with fiber-reinforced polymer composites”, *Journal of Constructional Steel Research*, 2012; 78, 131-143.

[6] Mao, X.Y. and Xiao, Y. "Seismic behavior of confined square CFT columns." *Engineering Structures*, 2006; 28(10), 1378-1386.

[7] Xiao, Y., He, W.H., and Choi, K.K. "Confined concrete-filled tubular columns." *Journal of Structural Engineering,* ASCE, 2005; 131(3), 488-497.

[8] Qin, P., Xiao, Y., Zhou, Y. and Zhang, G. “Research on CFRP confined circular concrete-filled steel tubular columns subjected to cyclic lateral forces”, *Journal of Earthquake Engineering and Engineering Vibration*, 2013; 33(5), 190-196.

[9] Gu, W., Guan, C.W., Zhao, Y.H., and Cao, H. "Experimental study on concentrically-compressed circular concrete filled CFRP-steel composite tubular short columns." *Journal of Shenyang Architecture and Civil Engineering University*, 2004; 20(2), 118-120, (in Chinese).

[10] Tao, Z., Han, L.H. and Zhuang, J.P. "Axial loading behavior of CFRP strengthened concrete-filled steel tubular stub columns." *Advances in Structural Engineering*, 2007; 10(1), 37-46.

[11] Wang, Z.B., Tao, Z. and Han, L.H. "Performance of CFRP-Strengthened concrete filled steel tubes under axial compression." *Proceedings, 10th International Symposium on Structural Engineering for Young Experts*, Hunan University, Changsha, China, 2008; 689-694.

[12] Liu, L. and Lu, Y.Y. "Axial bearing capacity of short FRP confined concrete-filled steel tubular columns." *Journal of Wuhan University of Technology-Materials Science Edition*, 2010; 25(3), 454-458.
[13] Park, J.W., Hong, Y.K. and Choi, S.M. "Behaviors of concrete filled square steel tubes confined by carbon fiber sheets (CFS) under compression and cyclic loads." *Steel and Composite Structures*, 2010; 10(2), 187-205.
[14] Abdalla, S., Abed, F. and Alhamaydeh, M. "Behaviour of CFSTs and CCFSTs under quasi-static axial compression", *Journal of Constructional Steel Research*, 2013; 90, 235-244.
[15] Wang Z.B., Yu, Q. and Tao, Z. "Behaviour of CFRP externally-reinforced circular CFST members under combined tension and bending", *Journal of Constructional Steel Research*, 2015; 106, 122-137.
[16] Hu, Y.M., Yu, T. and Teng, J.G. "FRP-confined circular concrete-filled thin steel tubes under axial compression", *Journal of Composites for Construction*, ASCE, 2011; 15(5), 850-860.
[17] Yu, T., Hu, Y.M. and Teng, J.G. "FRP-confined circular concrete-filled steel tubular columns under cyclic axial compression", *Journal of Constructional Steel Research*, 2014; 94, 33-48.
[18] Teng, J.G., Hu, Y.M. and Yu, T. "Stress-strain model for concrete in FRP-confined steel tubular columns", *Engineering Structures*, 2013; 49, 156-167.
[19] ASTM C192. *Standard Practice for Making and Curing Concrete Test Specimens in the Laboratory*, American Society for Testing and Materials, Philadelphia, USA, 2007.
[20] ASTM C39. *Standard Test Method for Compressive Strength of Cylindrical Concrete Specimens*, American Society for Testing and Materials, Philadelphia, USA, 2009.
[21] BS18. *British Standard Method for Tensile Testing of Metals*, British Standard Institution, 1987.
[22] ASTM D3039. *Standard Test Method for Tensile Properties of Polymer Matrix Composite Materials*, American Society for Testing of Materials, Philadelphia, USA, 2000.
[23] Boyd, P.F., Cofer, W.F., and McLean, D.I. "Seismic performance of steel-encased concrete columns under flexural loading." *ACI Structural Journal*, 1995; 92(3), 355-364.
[24] Iacobucci, R.D., Sheikh, S.A., and Bayrak, O. "Retrofit of square concrete columns with carbon fiber-reinforced polymer for seismic resistance." *ACI Structural Journal*, 2003; 100(6), 785-794.
[25] Susantha, K.A.S., Aoki, T., and Hattori, M. "Seismic performance improvement of circular steel columns using pre-compressed concrete-filled steel tube." *Journal of Constructional Steel Research*, 2008; 64(1), 30-36.
[26] Priestley, M.J.N., and Park, R. "Strength and ductility of concrete bridge columns under seismic loading." *ACI Structural Journal*, 1987; 84(1), 61-76.
[27] Chen, W.F., and Atsuta, T. *Theory of Beam Columns*, McGraw-Hill, New York, 1976.
[28] Park, R. "Evaluation of ductility of structures and structural assemblages for laboratory testing." *Bulletin of the New Zealand National Society for Earthquake Engineering*, 1989; 22(3), 155-166.
[29] Mirmiran, A., Shahawy, M., and Samaan, M. "Strength and ductility of hybrid FRP-concrete beam-columns." *Journal of Structural Engineering*, ASCE, 1999; 125(10), 1085-1093.
[30] Wu, Y.F., Liu, T., and Oehlers, D.J. "Fundamental principles that govern retrofitting of reinforced concrete columns by steel and FRP jacketing." *Advances in Structural Engineering*, 2006; 9(4), 507-533.
[31] Hu, Y.M. "*Behaviour and Modelling of FRP-confined Hollow and Concrete-filled Steel*

Tubular Columns," PhD thesis, Department of Civil and Structural Engineering, The Hong Kong Polytechnic University, Hong Kong, 2011.

[32] Gosain, N.K., Brown, R.H. and Jirsa, J.O. "Shear requirements for load reversals on RC members." *Journal of the Structural Division*, ASCE, 1977; 103(7), 1461-1475.

[33] Shim, C.S., Chung, Y.S., and Han, J.H. "Cyclic response of concrete-encased composite columns with low steel ratio." *Proceedings of the Institution of Civil Engineers-Structures and Buildings*, 2008; 161(2), 77-89.

Table

Table 1. Details of specimens

Specimen	D_{outer} ***(mm)***	t_s ***(mm)***	D_{outer}/t_s	t_{frp} ***(mm)***	***FRP type***	N_{app}/N_{sq}	N_{app} ***(kN)***	h_{frp} ***(mm)***
LCFT-0-106-E	318	3.0	106	N/A	N/A	0.35	1134	N/A
LCFT-5G-106-E				0.85	GFRP		1313	490
LCFT-0-106-F				N/A	N/A		1234	N/A
LCFT-5G-106-F				0.85	GFRP		1125	490
LCFT-6C-106-F				2.04	CFRP		1260	490

Table 2. Concrete properties

Specimen	f'_{co} ***(MPa)***	ε_{co}	E_c ***(GPa)***
LCFT-0-106-E	31.7	0.0027	21.7
LCFT-5G-106-E	37.0	0.0030	23.3
LCFT-0-106-F	35.6	0.0026	23.4
LCFT-5G-106-F	31.1	0.0026	21.9
LCFT-6C-106-F	36.6	0.0026	22.5

Table 3. Applied axial loads and calculated rolling frictional forces

Specimens	N_{app} ***(kN)***	***Calculated frictional force (kN)***	***Frictional coefficient***
LCFT-0-106-E	1134	5.95	0.00525
LCFT-5G-106-E	1313	6.95	0.00529
LCFT-0-106-F	1234	6.37	0.00516
LCFT-5G-106-F	1125	6.08	0.00540
LCFT-6C-106-F	1260	6.61	0.00525
		Mean	0.00527

Table 4. In-situ determined yield displacements

Specimen	δ_{y1} ***(mm)***	δ_{y2} ***(mm)***	δ_{y} ***(mm)***
LCFT-0-106-F	10.1	9.50	9.80
LCFT-5G-106-F	11.1	9.90	10.5
LCFT-6C-106-F	11.3	10.5	10.9

Table 5. Ductility ratios based on displacements

Specimen	δ_{y+}	δ_{u+}	$\mu_{\delta+}$	δ_{y-}	δ_{u-}	$\mu_{\delta-}$
CFT-0-106-E	10.20	48.67	4.77	N/A	N/A	N/A
LCFT-5G-106-E	11.70	65.83	5.63	N/A	N/A	N/A
LCFT-0-106-F	10.27	55.90	5.44	11.08	62.61	5.65
LCFT-5G-106-F	10.91	58.45	5.35	10.33	66.07	6.39
LCFT-6C-106-F	11.29	70.98	6.29	10.93	96.88	8.86

Figure

Click here to download Figure: Cyclic_Lateral_Tests_Figures_V2.docx

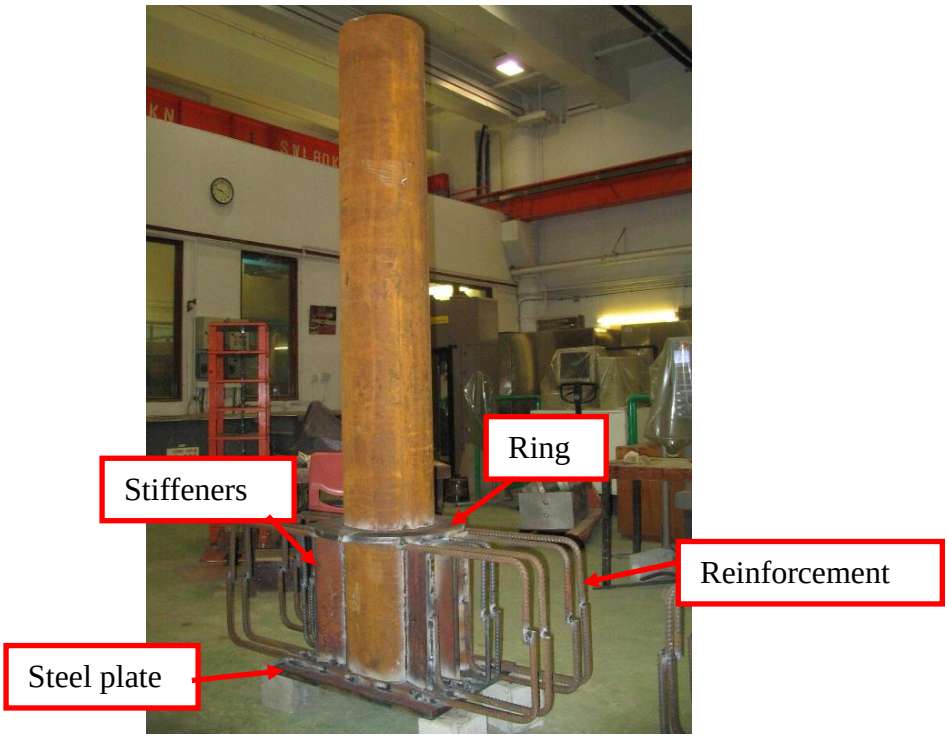

Figure 1. Reinforcement details in the footing

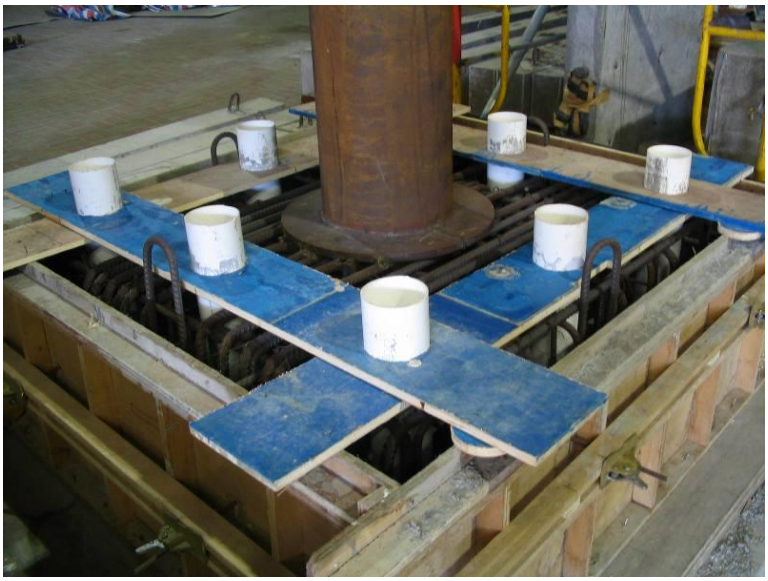

Figure 2. Specimen ready for concrete casting

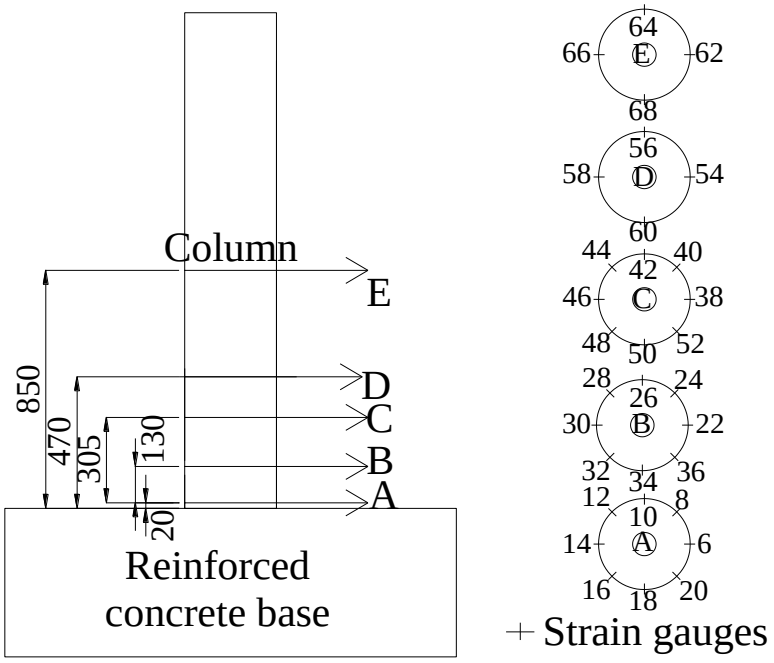

(Dimensions in mm)

Figure 3. Layout of strain gauges

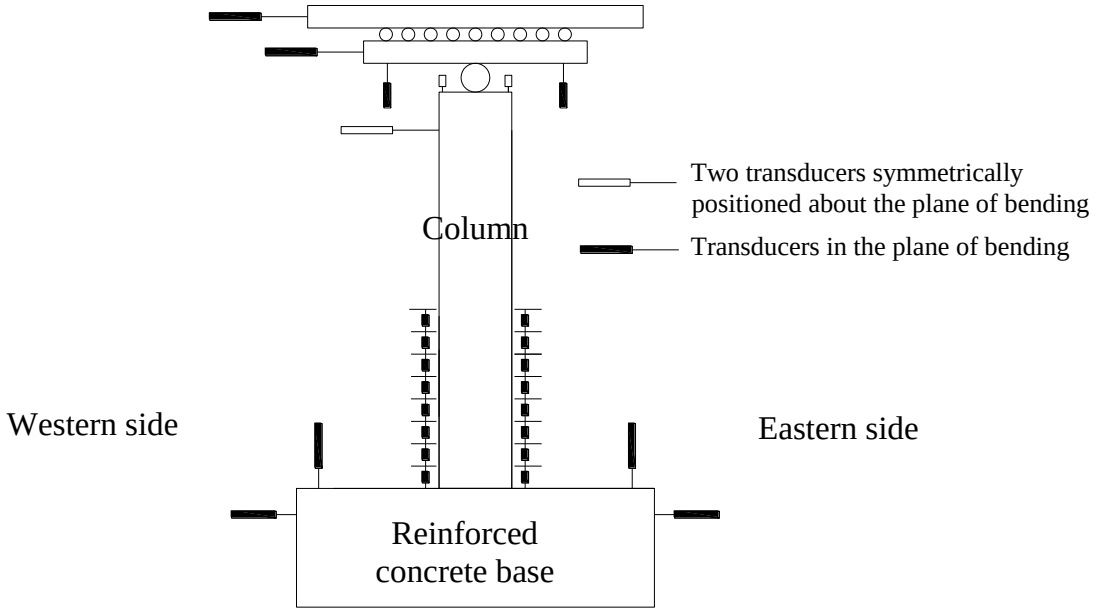

Figure 4. Layout of transducers

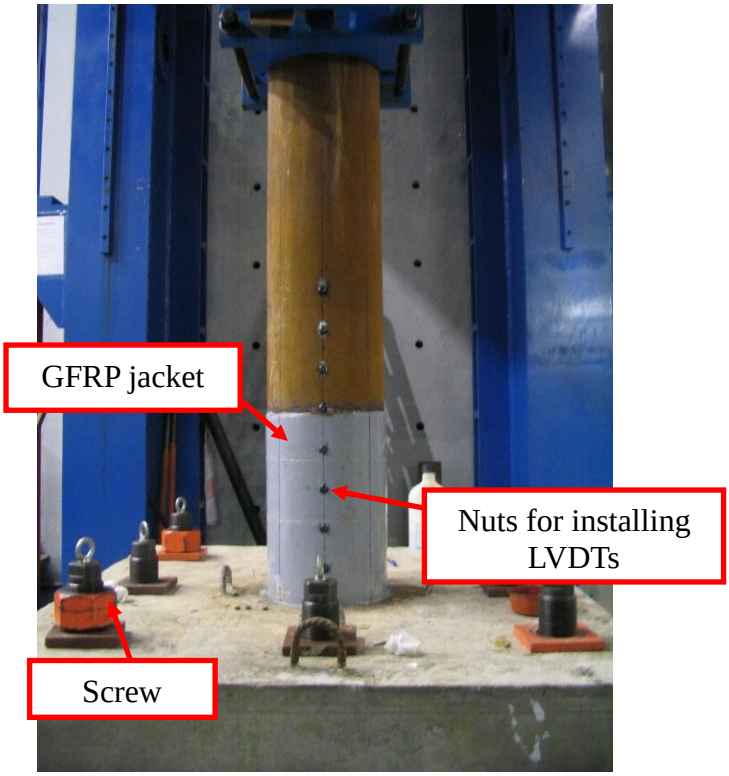

Figure 5. Column wrapped with a GFRP jacket

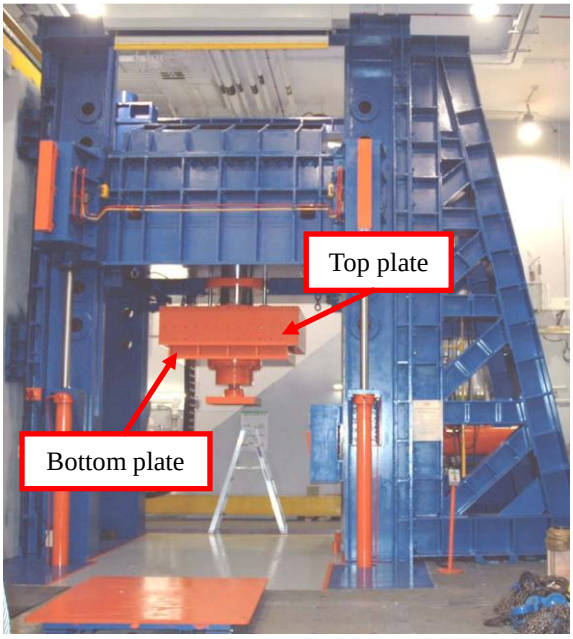

Figure 6. Testing frame

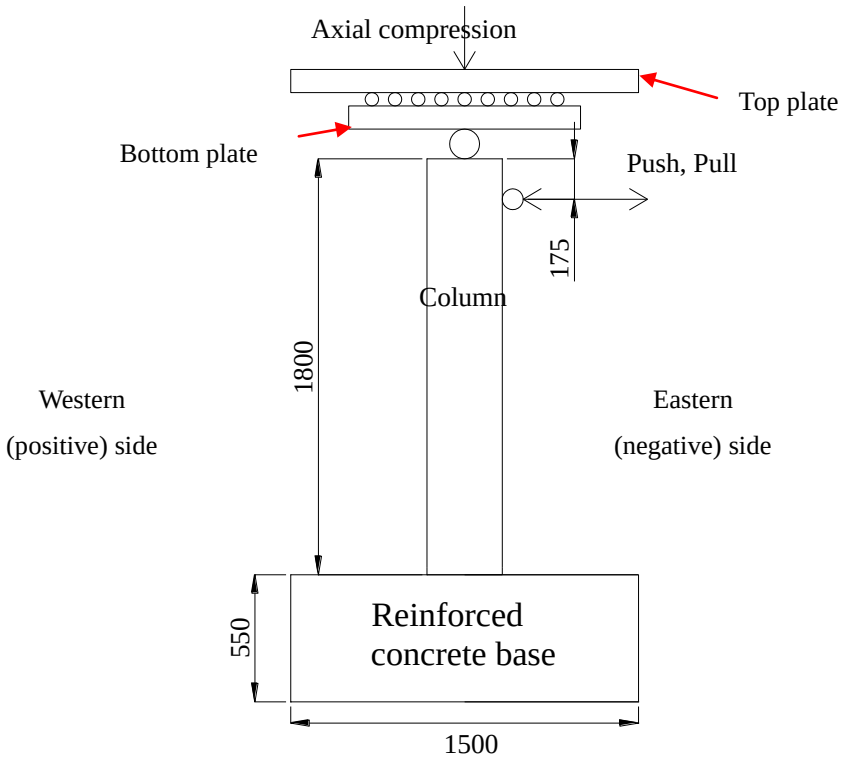

Figure 7. Schematic diagram of test set-up

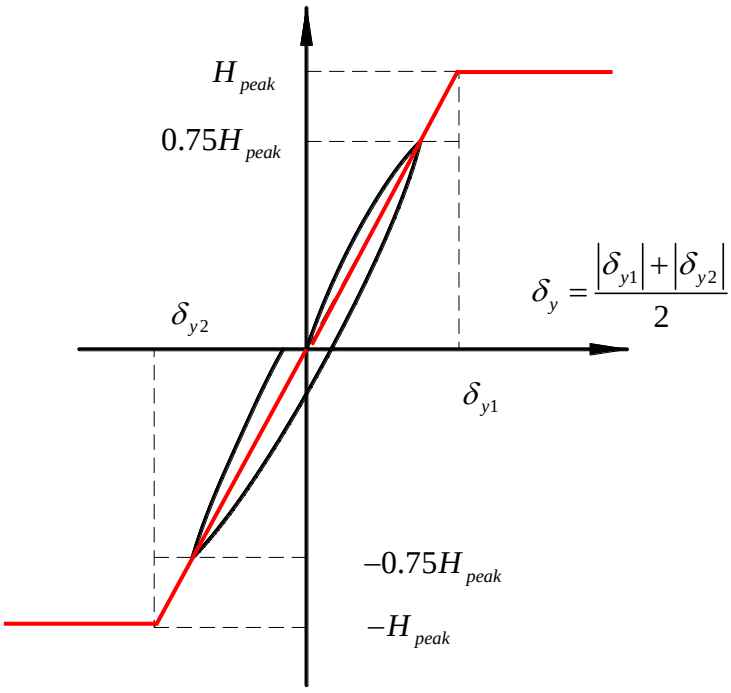

Figure 8. Experimental definition of yield displacement

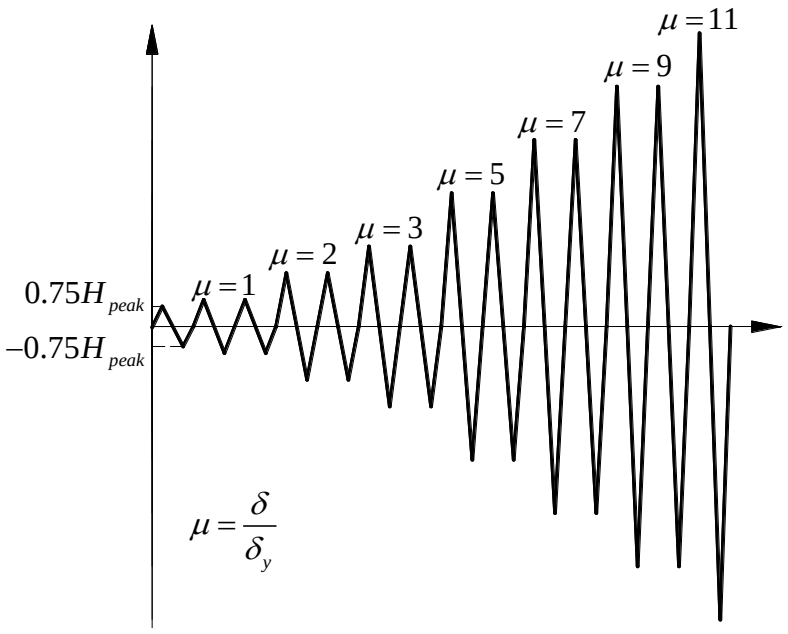

Figure 9. Applied lateral displacement history

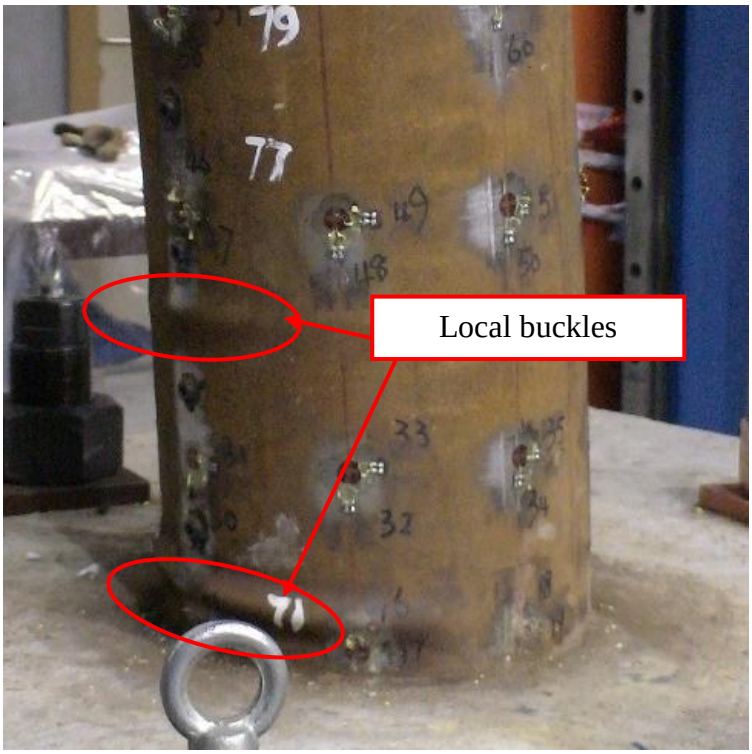

(a) Specimen LCFT-0-106-E

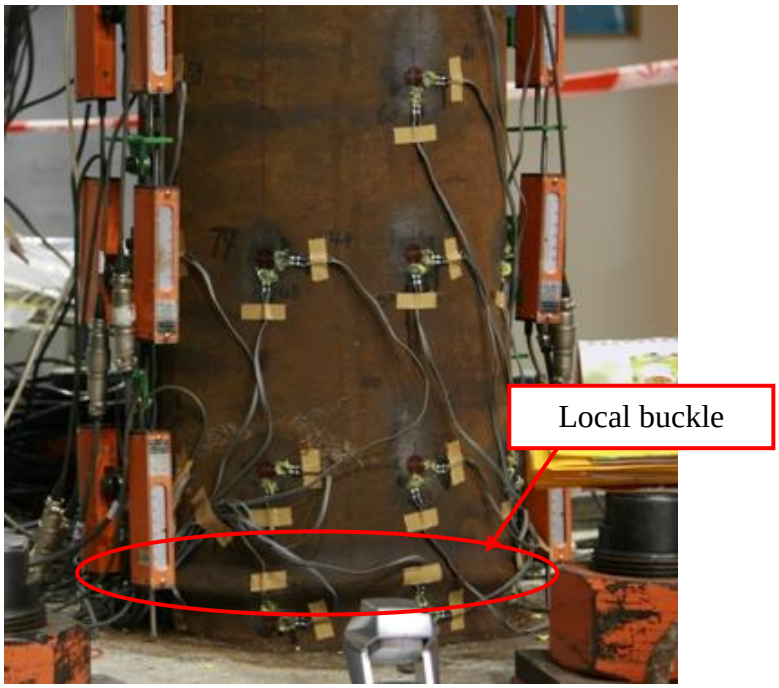

(b) Specimen LCFT-0-106-F

Figure 10. Outward local buckling of steel tube in CFT specimens

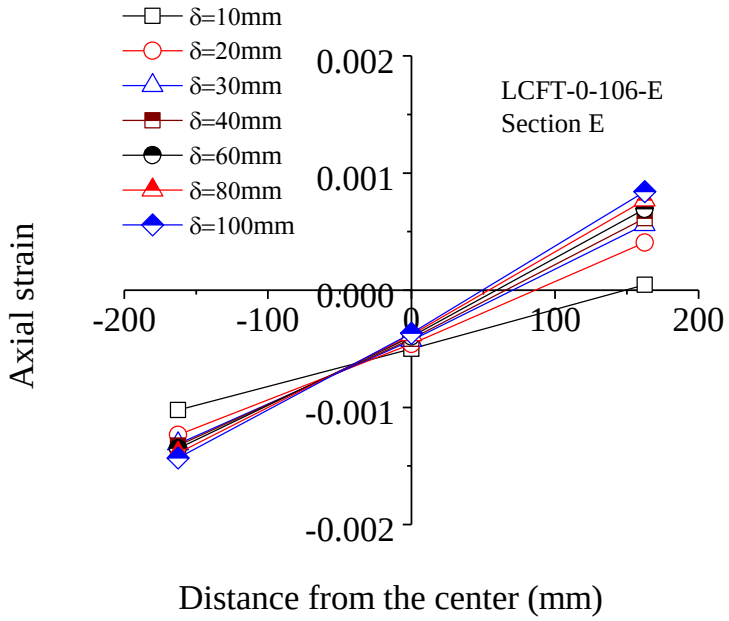

(a) Section E

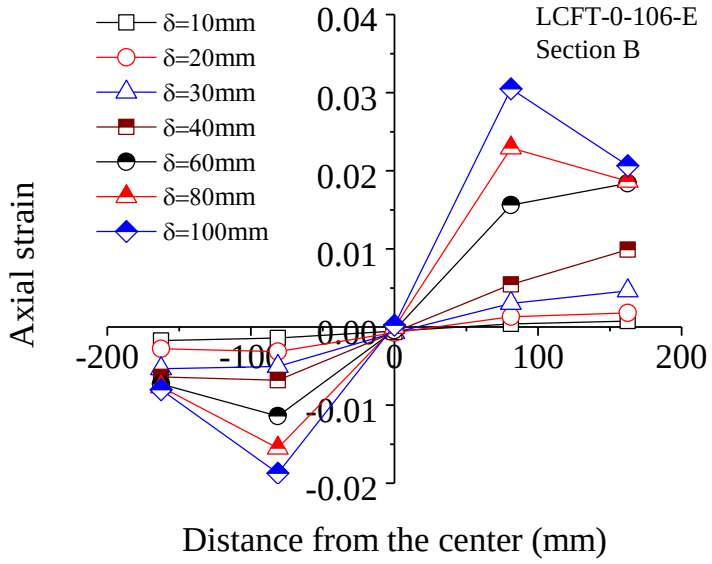

(b) Section B

Figure 11. Axial strain distributions in column LCFT-0-106-E

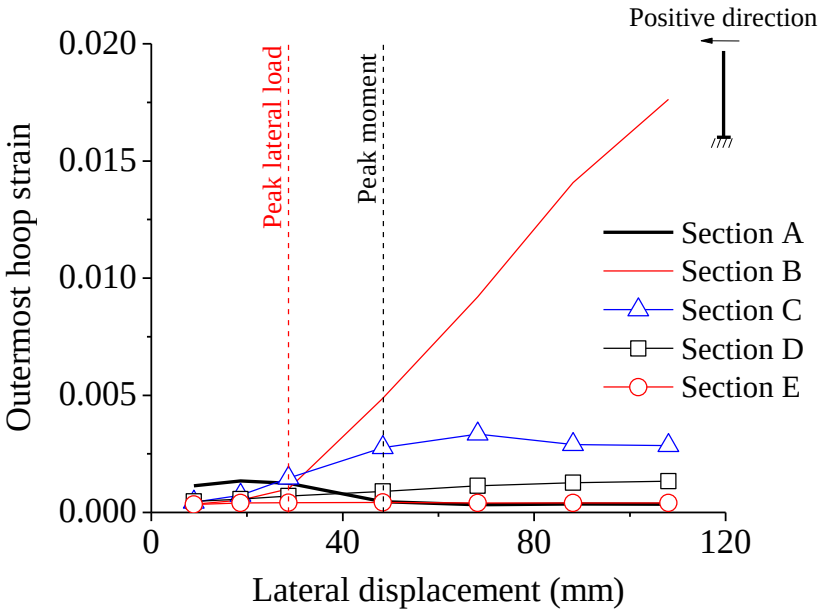

(a) Specimen LCFT-0-106-F

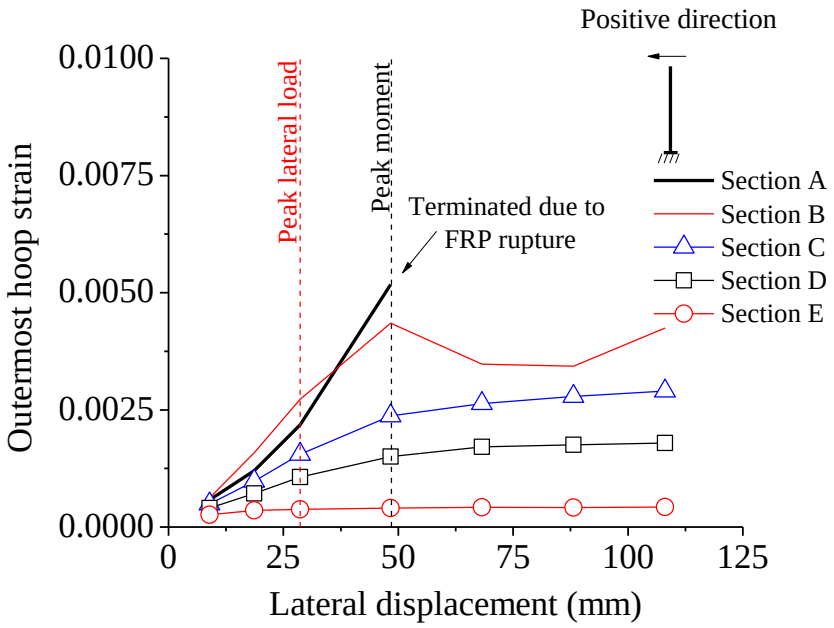

(a) Specimen LCFT-5G-106-F

Figure 12. History of hoop strains of extreme compression fibre

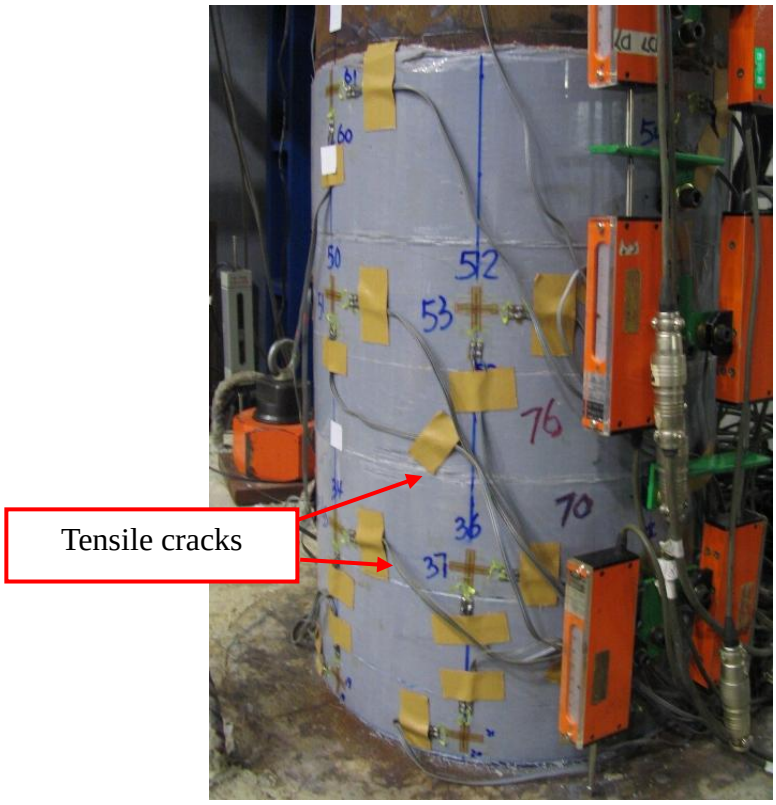

(a) Column LCFT-5G-106-E

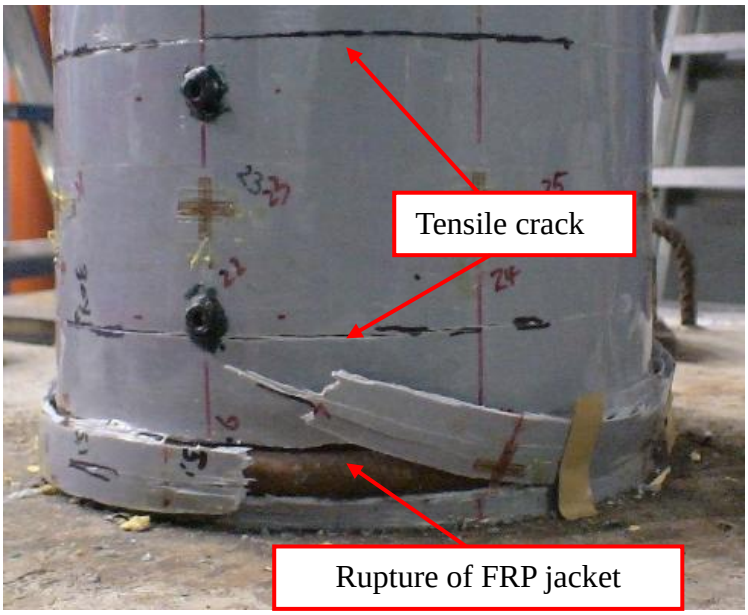

(b) Column LCFT-5G-106-F

Figure 13. Failure mode of CCFTs with a 5-ply GFRP jacket

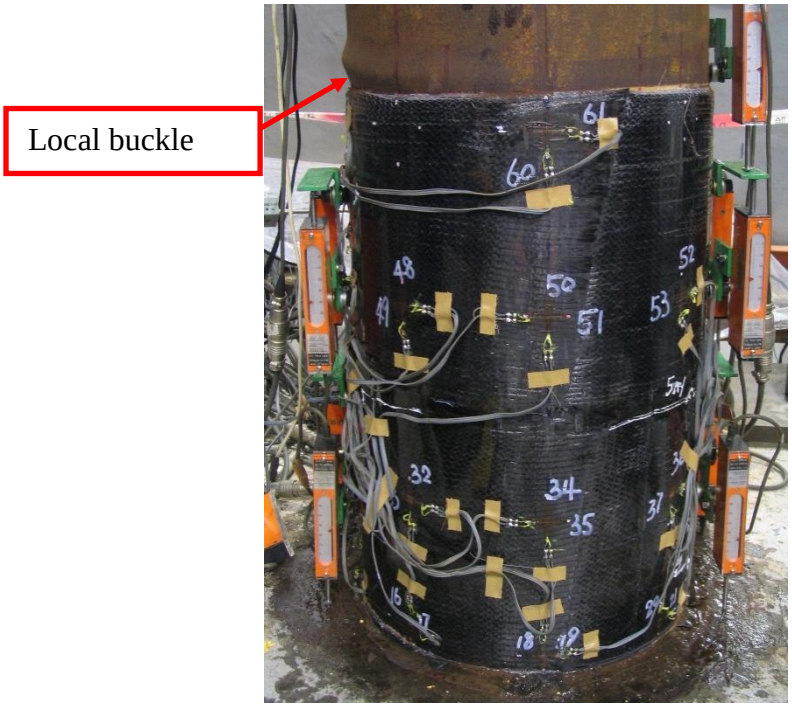

Figure 14. Column LCFT-6C-106-F after test

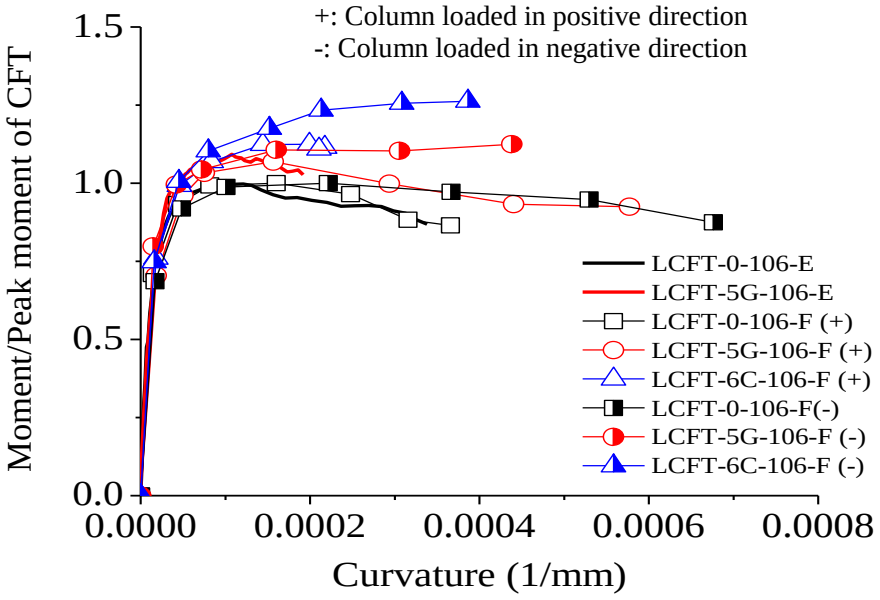

Figure 15. Normalized moment-curvature curves of all specimens

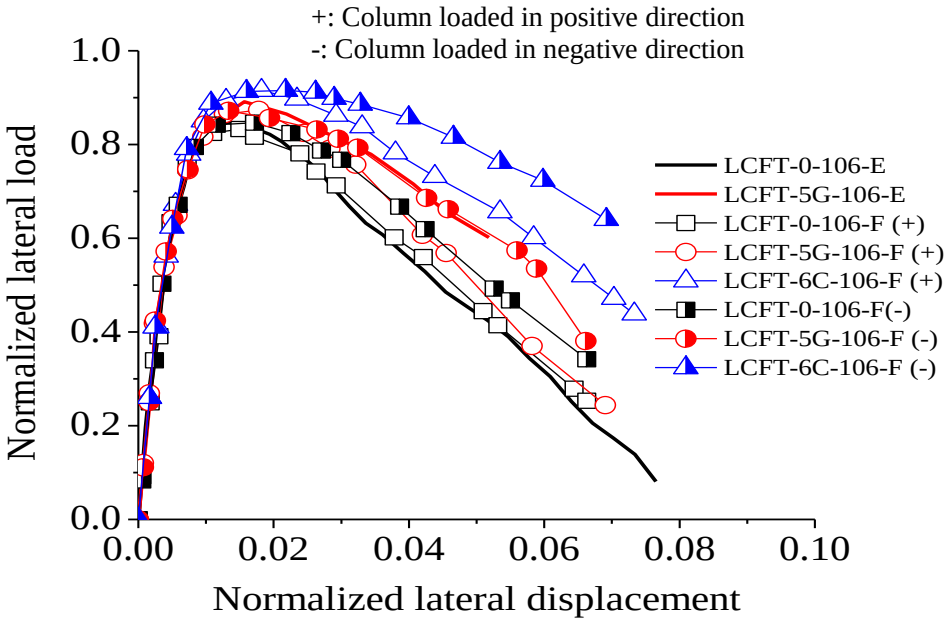

Figure 16. Normalized load-displacement curves of all specimens

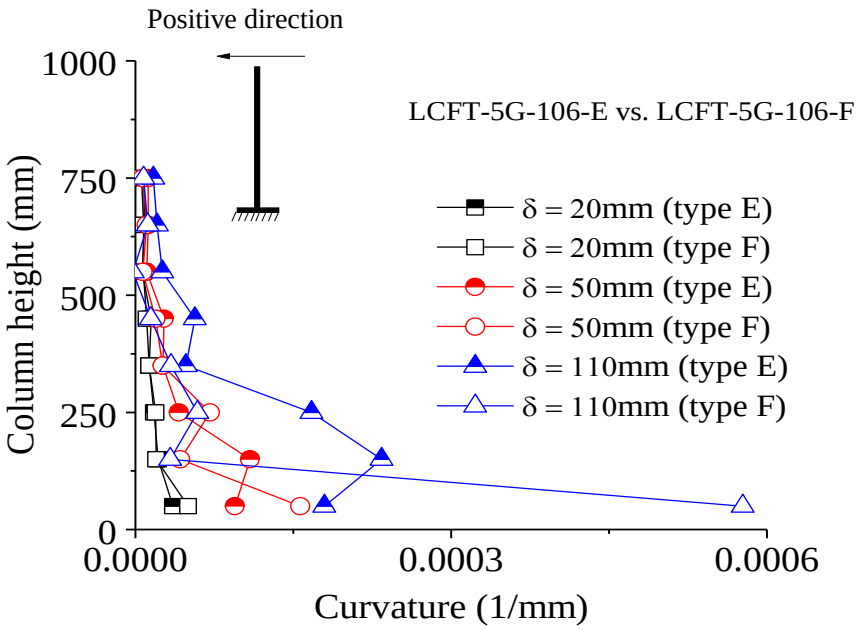

Figure 17. Curvature distributions in GFRP-confined columns

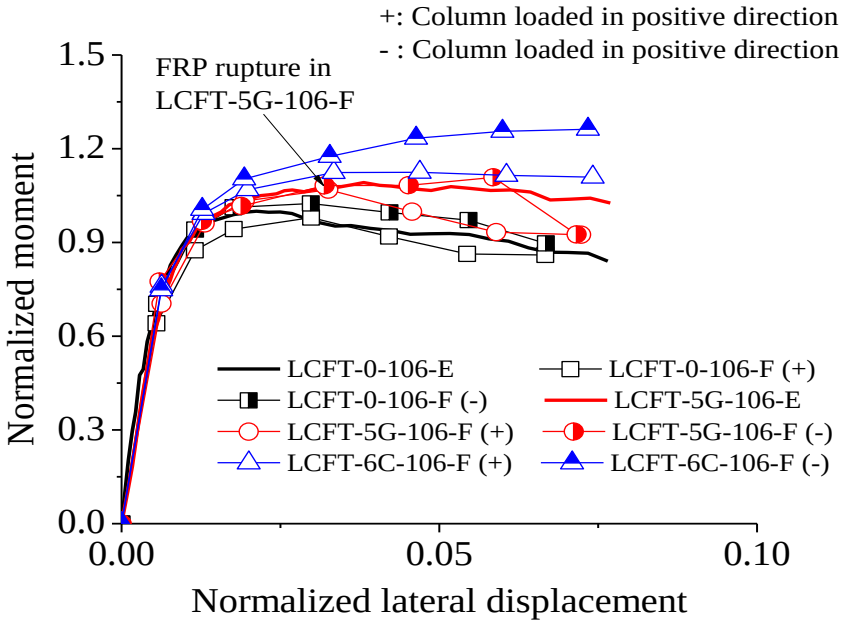

Figure 18. Normalized moment-displacement curves

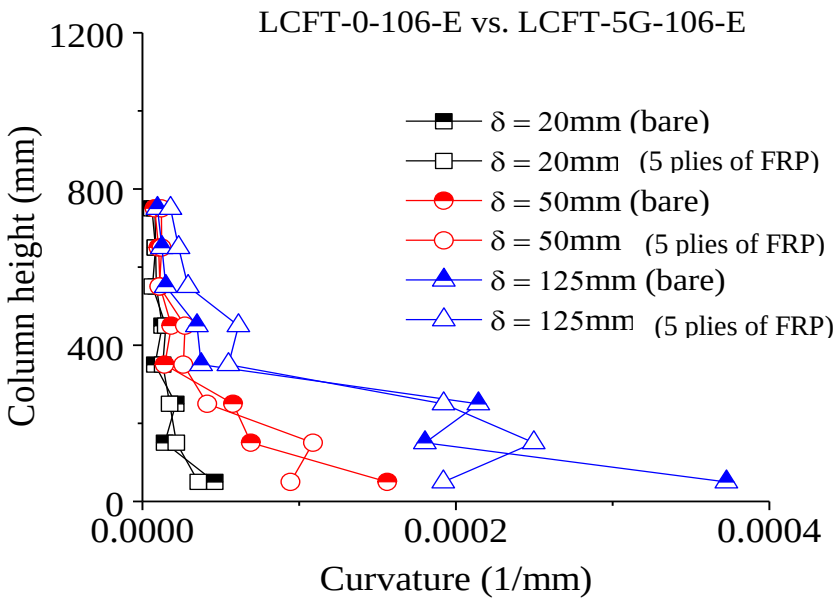

Figure 19. Curvature distributions in columns under monotonic lateral loading

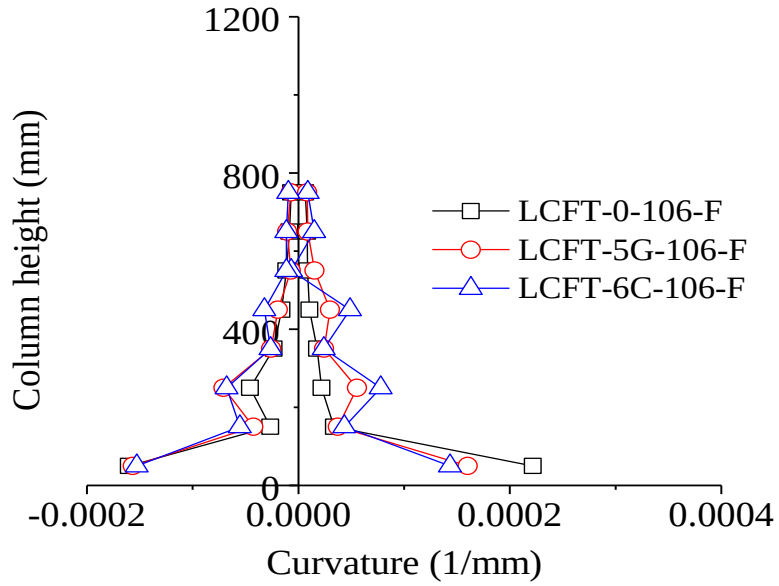

(a) δ =+/-50mm

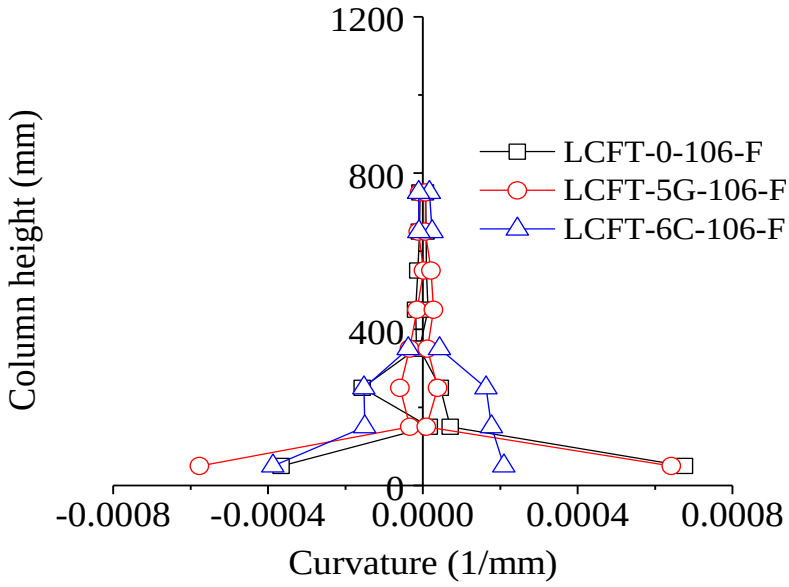

(b) δ =+/-110mm

Figure 20. Curvature distributions in columns under cyclic lateral loading

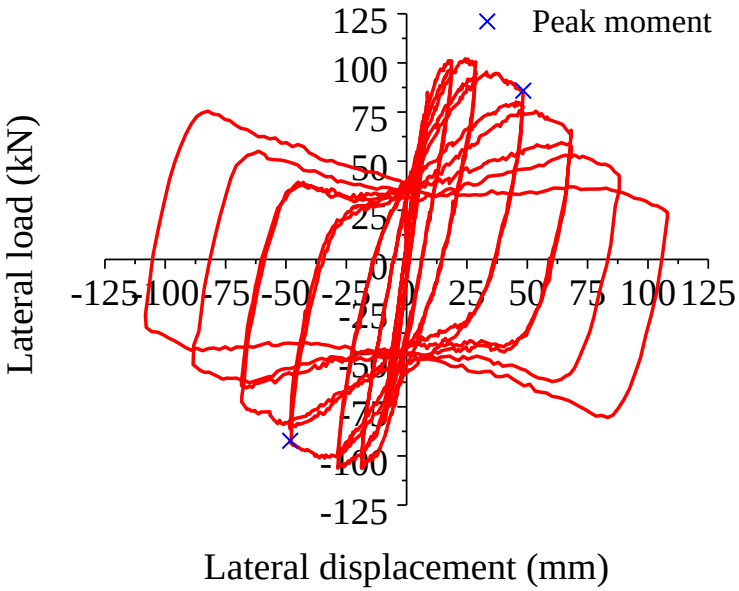

(a) Specimen LCFT-0-106-F

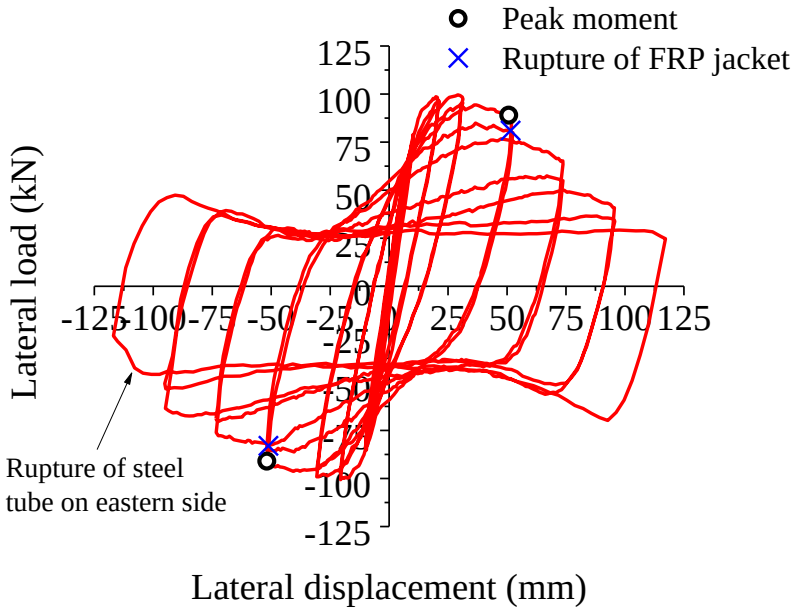

(b) Specimen LCFT-5G-106-F

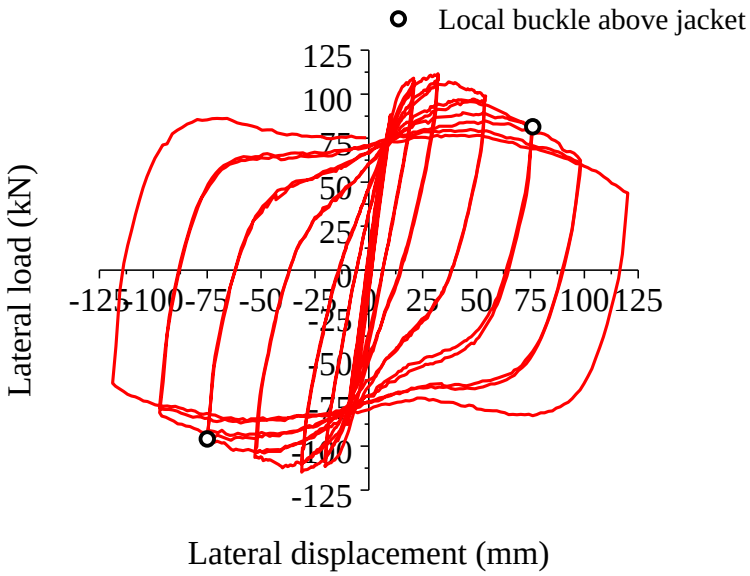

(c) Specimen LCFT-6C-106-F

Figure 21. Hysteristic load-displacement curves